Electronic Supplementary Material (ESI) for Journal of Materials Chemistry C

Supplementrary Information

"Catalyst-free growth of readily detachable nanographene on alumina"

Jaehyun Park, [ab] Kyung Hoon Kim, [a] Joonsung Kim, [a] Cheol Jin Lee, [c] Joon Hyung Shim, [d] Yong-Won Song,*[b] and Jeong Sook Ha*[ae]

[a] *Department of Chemical and Biological Engineering, Korea University, 5-1 Anam-dong, Seoul 13l-701, Korea. E-mail: jeongsha@korea.ac.kr*

[b] *Future Convergence Research Division, Korea Institute of Science and Technology, Hwarangno 14-gil 5, Seoul 136-791, Korea. E-mail: ysong@kist.re.kr*

[c] *School of Electrical Engineering, Korea University, 5-1 Anam-dong, Seoul 13l-701, Korea.*

[d] *Department of Mechanical Engineering, Korea University, 5-1 Anam-dong, Seoul 13l-701, Korea.*

[e] *KU-KIST Graduate School of Converging Science and Technology, 5-1 Anam-dong, Seoul 13l-701, Korea.*

We can grow graphene (Gr) on various substrates, including Cu, Ni, SiO_2, Al_2O_3, and ZrO_2 under the same conditions via thermal CVD. We exhibited the representative Raman spectra of graphene on three kinds of substrates (**SI 1a**). Gr on Cu exhibits grain size up to several μm. Gr on SiO_2 also exhibited nano-size grain at the initial growth, but at the growth time of 15 min, it showed film-like grain as shown in **SI 1b**.

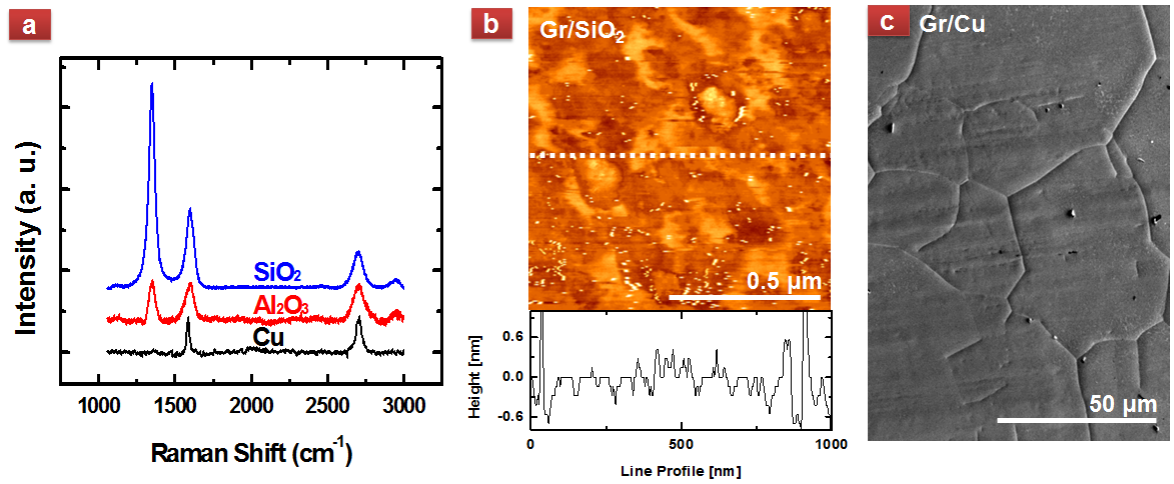

SI 1. (a) Raman Spectra of as-grown graphene (Gr) on Cu, Al_2O_3, and SiO_2 substrate. Under the same growth conditions, graphene was synthesized on Al_2O_3 and SiO_2. For the growth of graphene on Cu, temperature was elevated in H_2 atmosphere. (b) AFM image of Gr on SiO_2, (c) SEM image of Gr on Cu.

In order to optimize the growth conditions on Al_2O_3, the growth temperature and the ambient gases were varied. The left scheme of **SI 2** shows the supply of gas flow in accordance with the elevation of temperature. As shown in the Raman spectra, the quality of the grown graphene film was strongly dependent on the ambient gas species. Under Ar or H_2 atmosphere, similar Raman spectra were obtained, but the nGr under Ar atmosphere showed lower defect density with a smaller I_D/I_G ratio. However, nGr grown under dilute H_2O gases produced a much thicker nGr film indicating higher growth rate, which is similar to the super-growth of SWCNTs on Al_2O_3 under H_2O atmosphere.

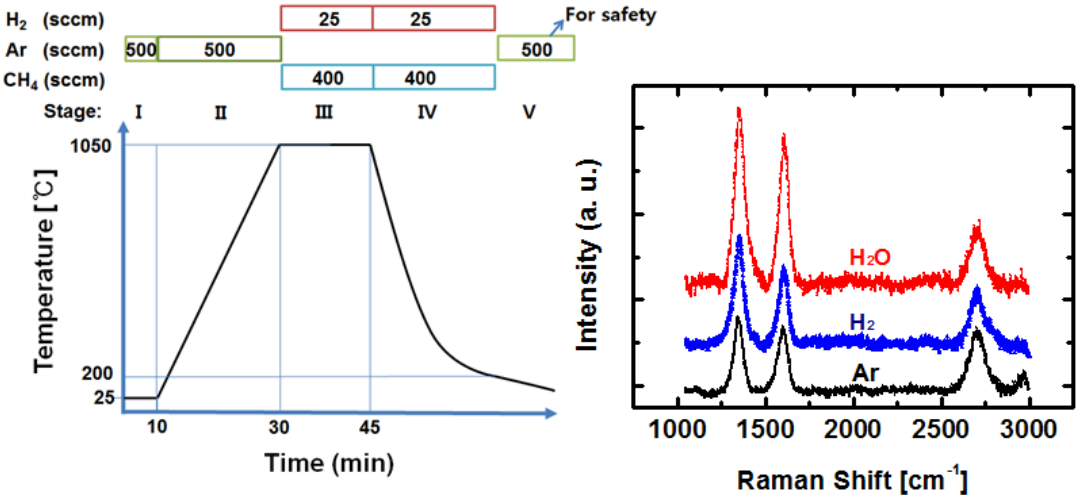

SI 2. (Left) Optimized gas feeding in accordance with the heating of Al_2O_3 substrate. (Right) Raman spectra taken from nGr films on Al_2O_3 under different gas atmospheres during the heating of the substrate indicated as the stage II in the left temperature-time plot. From the bottom, spectra of nGr grown under Ar, H_2, and Ar with a small amount of H_2O, respectively.

Analysis of dome structure of nGr

In the early stage of the nGr growth, hemispherical domes form as nuclei. As the growth proceeds, the domes become planar grains via lateral growth along the substrate surface. On encountering the other grains, the areal expansion is limited and the up-convex grains are formed for storing strain energy. This feature would happen more easily if the grown grains have low affinity with the substrate. At the critical point, a dome would collapse by forming node-like sub-domes, which would be ripples. During the growth, the grains would be merged into larger ones to reduce the total strain energy. From a thermodynamic perspective, the length of grain boundaries (GB) would be decreased to reduce the system energy, which produces isotropic grains. Pits are from the grain-free surface areas (see **Figure 1a**). The nGr domes, the ripples, the latent grain boundaries (LGB), and the pits can be observed in the AFM image.

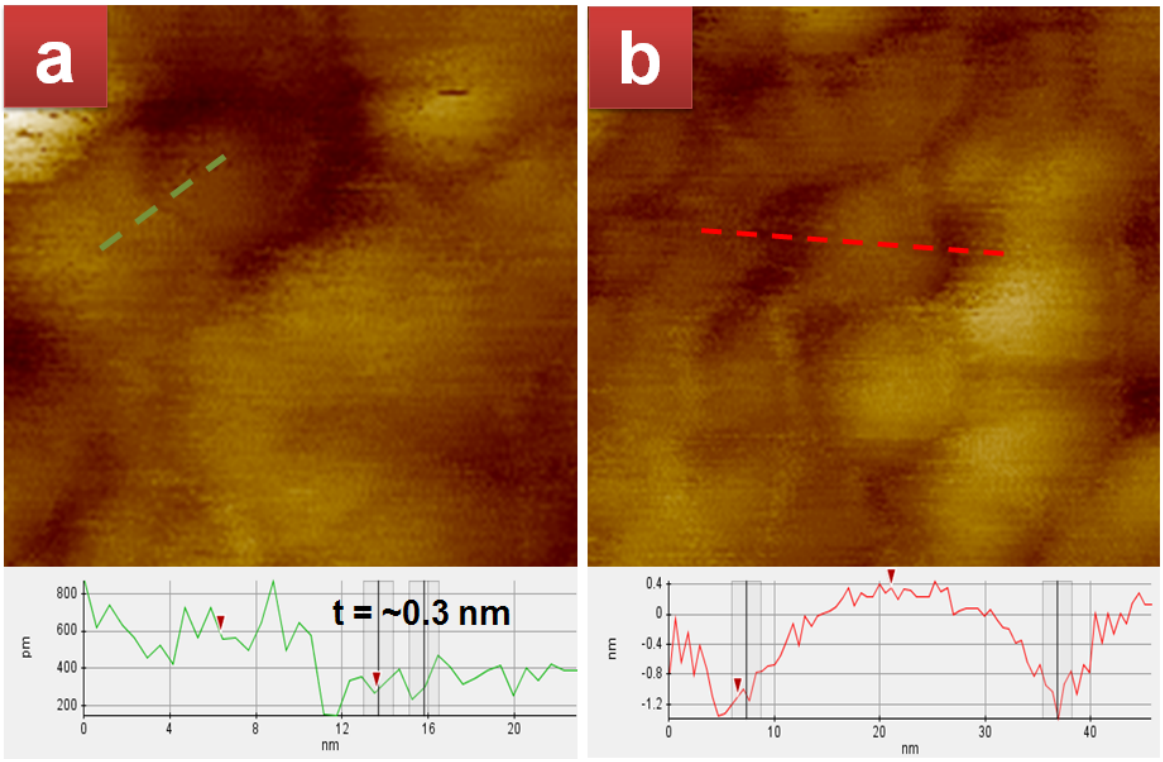

SI 3. (a) and (b) are partly magnified AFM images and line profiles of Figure 1(a). Line profile of (a) shows the height difference of ~0.3 nm (left half is double-layered nGr and right half is monolayered nGr), which is comparable to the thickness of monolayered graphene. (b) is a representative dome structure made of nGr, and its line profile.

To estimate the structural stability and the detaching feasibility of the grown nGr dome on Al_2O_3 substrate, we selected a representative dome as shown at **SI 4b**. Consequently, the adsorption energy of graphene on Al_2O_3 is ~20 times smaller than that on SiO_2. This feature would guarantee the successful dry-transfer method for detaching the graphene grown on Al_2O_3 substrate.

For the quantitative analysis, we assumed the outline of the dome as a circular arc with radius r and subtending angle α (rad). There are two simple geometrical relationships,

(1) $\cos \alpha = 1 - (d/L_a)\,\alpha$, (2) $r = (L_a/2)/\alpha$, where d is 1.4 nm, $L_a/2$ = 14.6 nm.

From these two simple relationships, we can get the solutions, r = ~150 nm, and α = 0.1 rad.

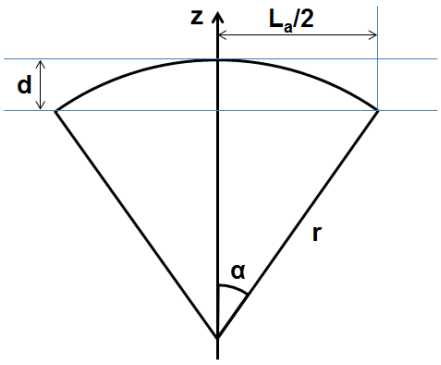

SI 4. Graphical illustration of nGr dome as a part of circular sector with r as the radius of the circle, and α as the half of the central angle. A diameter and a height of a nGr dome are L_a and d, respectively. The chord corresponds to the surface of Al_2O_3 substrate.

This dome structure such as the intrinsic ripples in normal graphene can be maintained via contact force characterized by a surface tension, r_S and an elastic energy that was induced as in-plane stress.

The Young's modulus[1] in linear elasticity can be defined as

$$E_{2D} = \frac{4\,\mu\,(\mu+\lambda)}{2\mu+\lambda} \qquad (3)$$

, where λ is Lamé's first parameter, and μ is the shear modulus or Lamé's second parameter. These two Lamé coefficients of graphene at room temperature were evaluated by quasiharmonic approximation; μ is 10 eV/Å^2, and λ is 2 eV/ Å^2.[2] Based on these two values, we can evaluate the E_{2D} = 21.8 eV/ Å^2.

The elastic energy due to in-plane strains[1] can be roughly defined by

$$E_{el} \sim \frac{d^4}{{L_a}^2} E_{2D} \quad (4)$$

, where d is the height fluctuation of 1.4 nm, and L_a is the chord length of 29.2 nm. The evaluated E_{el} is 9.82 eV.

The bending energy[1] can be defined as

$$E_k = \kappa \frac{d^2}{{L_a}^2} \quad (5)$$

, where κ is the bending rigidity of 1.17 eV.[3]

From this equation, the E_k applied at the nGr dome is only 2.7 meV.

The surface area of the nGr dome is ~695 nm^2, and its projected area is ~669 nm^2. Therefore, the difference between the surface area and its projected area of the dome is only ~26 nm^2. The equivalent carbon atoms added for forming dome structure is, therefore, 26 nm^2 / (5.2 Å^2/ 2 carbon atoms) = 1000 carbon atoms. (The lattice spacing and the area of the unit cell (honeycomb lattice) of graphene are 1.42 Å and 5.2 Å^2, respectively.) By forming the dome structure, the relieved adsorption energy can be evaluated as ~2.6 eV (2.6 meV/carbon on Al

terminated (0001) surface of Al_2O_3[4] × 1000 carbon). This calculation can conclude that the applied bending energy is very small. Therefore, the lattice spacing of the unit cell of graphene can be neglected.

In the grain analysis of the AFM images, we could evaluate that the portion of nGr dome is conservatively ~0.7 by using height threshold method in XEI program (Park Systems). The other portion, 0.3 was used for the pinning energy, E_{pin},[1] which grabs the dome,

$$E_{pin} \sim \gamma_s A^2 \quad (6)$$

, where A^2 is the pinning area of ~287 nm^2.

Consequently, the E_{pin} is 29 eV. This energy is 10^4 time higher than E_k. This can be concluded that the nGr structure is stably attached on the surface of Al_2O_3 substrate.

This kind of nGr dome structure is beneficial for peeling-off the grown graphene. From Cuong's report, the adsorption energy of graphene on SiO_2 is 15 meV/carbon atom, which is the energy level of most stable adsorption state. This indicates a weak interaction between graphene and SiO_2 (0001) surfaces.[5] However, the energy of graphene on Al_2O_3 is 2.6 meV/carbon atom, which is ~6 times smaller. Moreover considering the effective adsorbing area onto Al_2O_3 surface considering the dome structure, the energy on Al_2O_3 is ~20 times smaller than that on SiO_2. This feature would guarantee the successful dry-transfer method for detaching the graphene grown on Al_2O_3 substrate.

In the aspect of the coupling strength between two graphene layers in graphite is 52~78 meV/carbon atom.[6] These values are 20~30 times smaller than the strength between graphene and Al_2O_3 (2.6 meV/carbon atom). Considering the dome structure, the difference of the

strengths would be dramatically increased. Even though the grown graphene is mulilayered one, this would be transferred perfectly without the Gr-Gr layer separation.

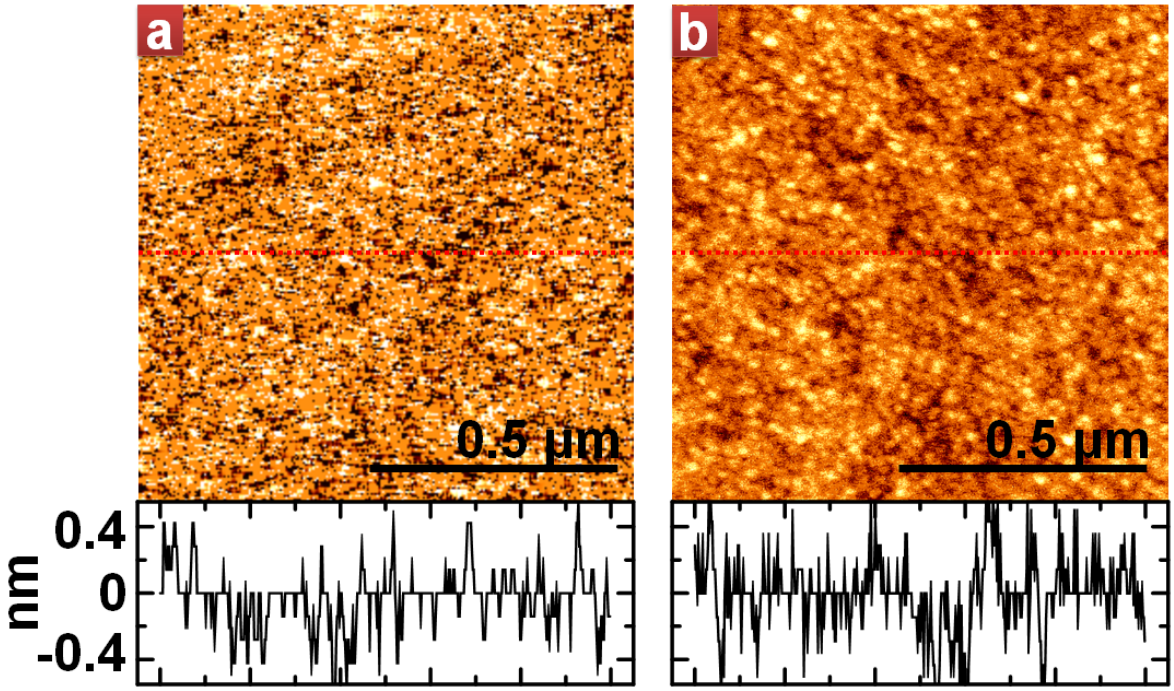

SI 5. Representative AFM images and line plots of ALD grown Al_2O_3 surfaces. (a) A finely controlled flat surface, and (b) a rough surface depending on the ALD growth conditions.

Electrical characteristics of nGr TFTs

In order to open a band gap in graphene, many different methods have been suggested, including chemical reactions to destroy the honeycomb structure, cutting into small-sized graphene pieces by lithographic techniques, unzipping CNTs, a direct synthesis to yield quantum effects, growing bilayer graphene, appropriate selection of substrate or dielectric layer, and formation of bent structures by strain.[7-9] The band gap should be higher than 0.5 eV for the operation of graphene devices at room temperature.[7] Therefore, graphene-channel widths of 2~3 nm for the monolayer[7] and <10 nm for the bilayer should be obtained.[9] It was also reported that Al-terminated and hydroxylated surfaces also contribute to the band gap opening by 138 and 126 meV, respectively.[8] Moreover, additional strains can also contribute, as shown in **Figure 3b**. Considering especially the size effects, our polycrystalline nGr is expected to open the band-gap more easily than graphene nanoribbons. Even though the Dirac point was not observed, a clear difference in the on/off current ratio between the FETs using nGr grown for 15 and 20 min was measured, which can be an indirect evidence of band-gap opening.

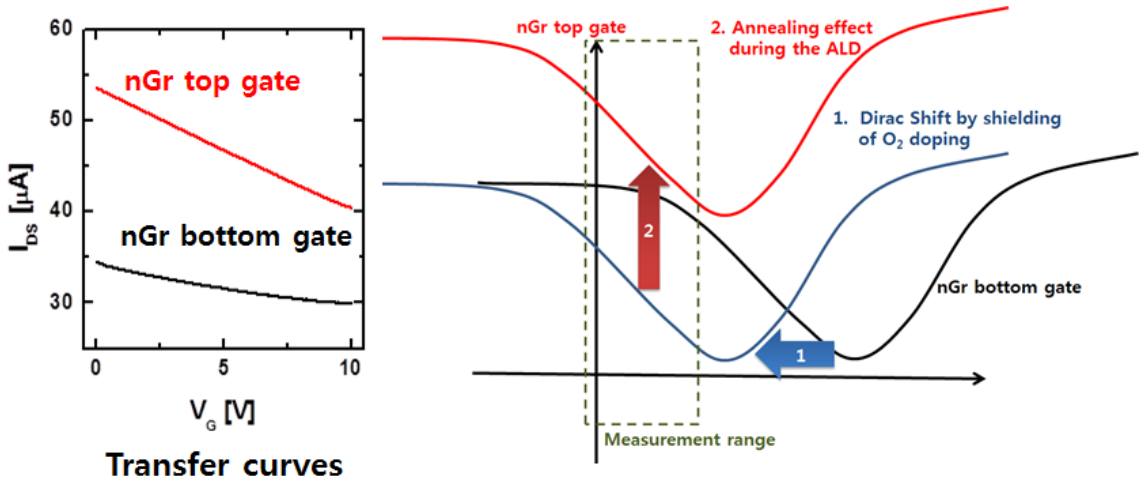

SI 6. (Left) transfer curves of the top-gate and bottom-gate nGr FETs. (Right) imaginary transfer curves expected to be varied by the ALD of Al_2O_3 top gate dielectric film. 1 and 2 are the shifts of the curve toward the left due to dedoping by passivation, and upward due to improved contact resistance by annealing, respectively.

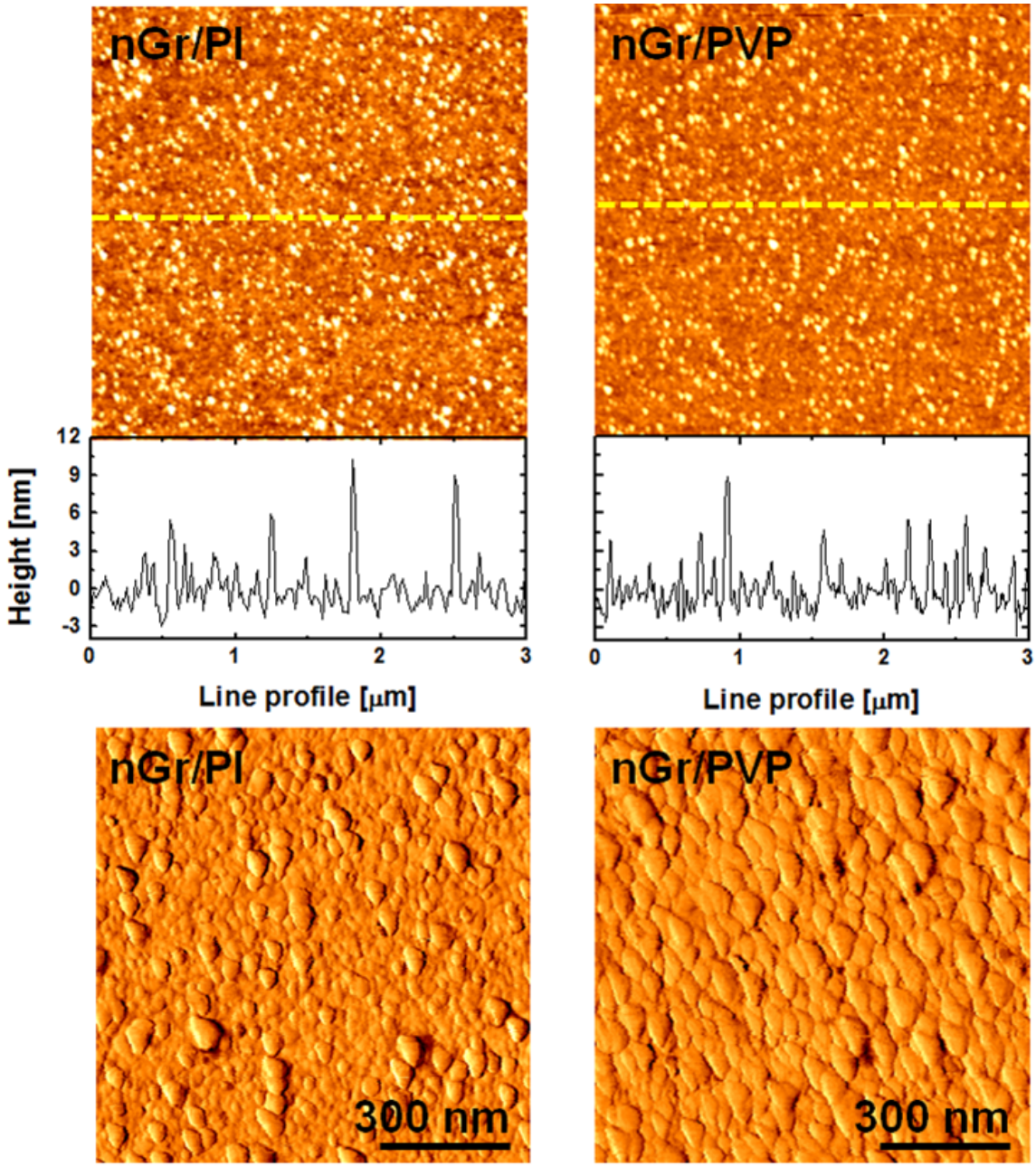

SI 7. AFM (top) and LFM (bottom) images of nGr on PI and PVP, respectively. Root mean square roughness values of nGr film on PI and PVP were 2.2 and 1.6 nm, respectively.

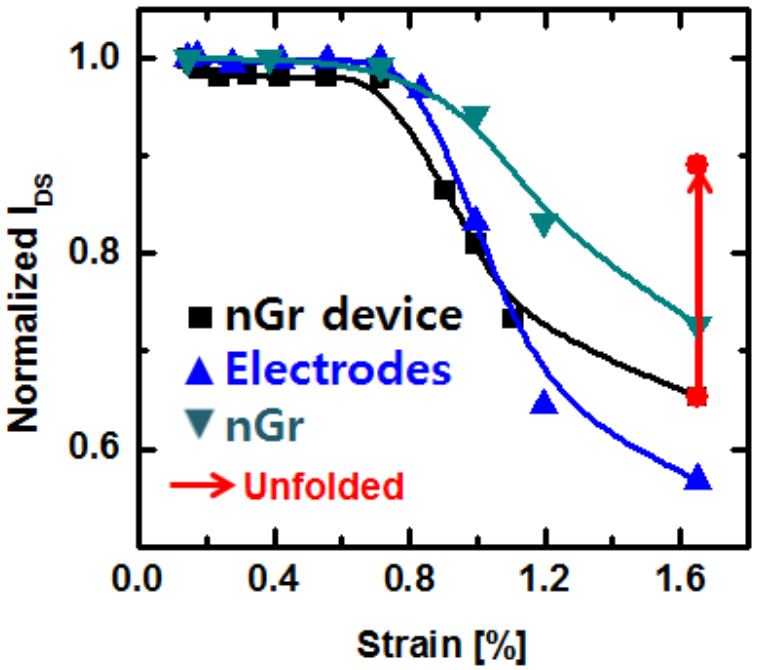

SI 8. Change of normalized current upon corresponding strain. Squares, triangles, and inverse triangles represent the current of nGr device, electrodes, and nGr on 200 μm thick PI/thermal release tape.

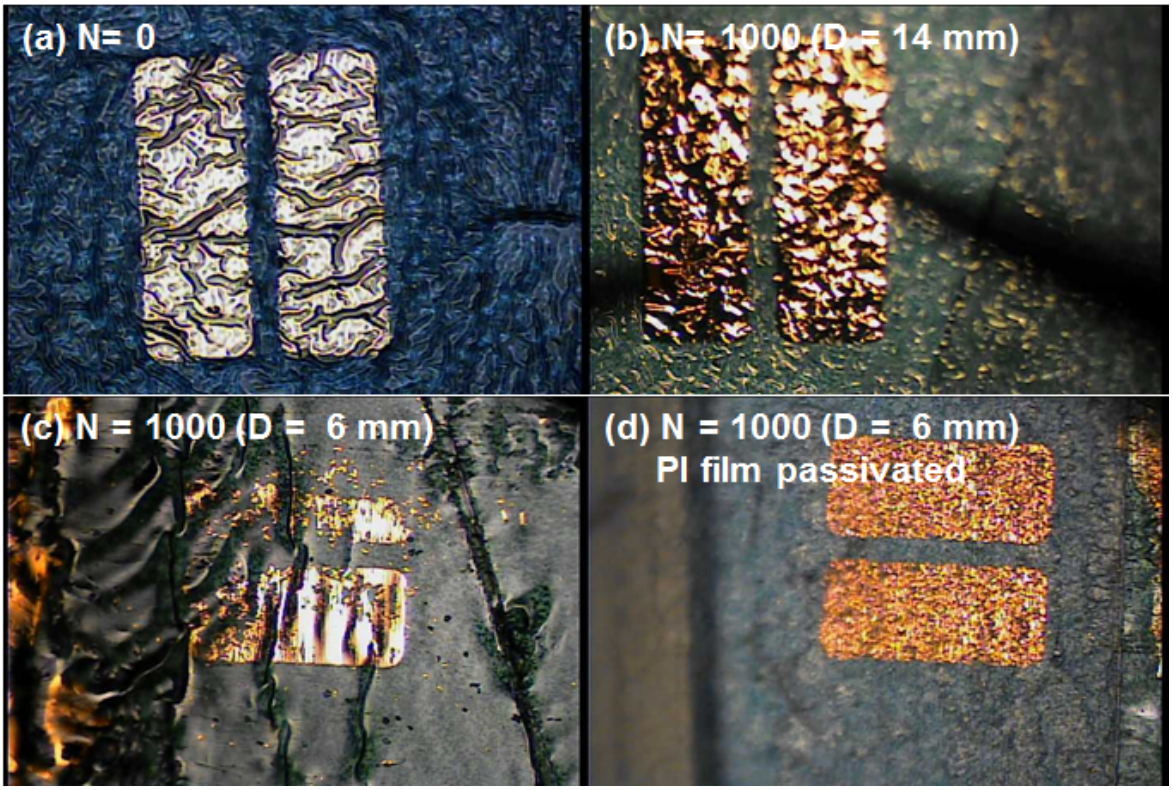

SI 9. Optical microscope images of electrodes after repetitive bending with the number of bending cycles (N). (a) No bending and N=1000 under bending diameter (D) of (b) 14 mm and (c) 6 mm. (d) N=1000 and D= 6 mm, with electrodes passivated by PI film.

Fabrication process of nGr top-gate TFTs

1. ALD growth of 50 nm thick Al_2O_3 film on thermally grown 300 nm thick SiO_2/Si substrate.
2. Growth of nGr film on Al_2O_3

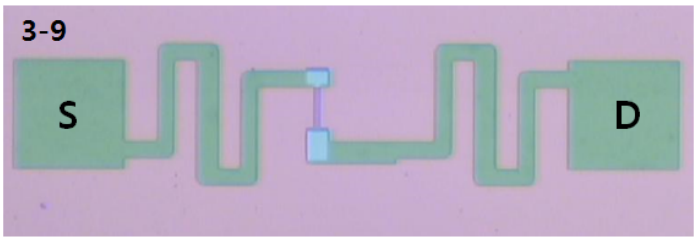

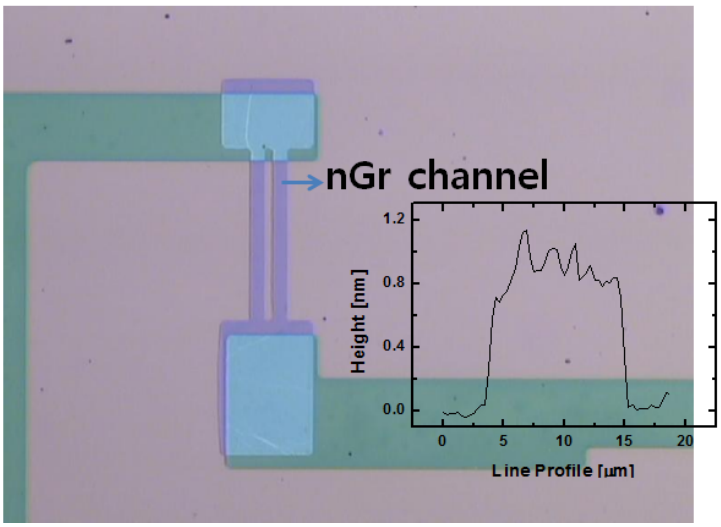

3. Photolithography for forming the patterns of S-D electrodes
4. E-beam evaporation for forming S-D electrodes (30 nm Au/3 nm Ti)
5. Lift-off
6. Photolithography for forming the patterns of nGr channels
7. O_2-RIE
8. Removing the residual PR
9. ALD growth of 50-nm thick Al_2O_3 film for forming gate-dielectric

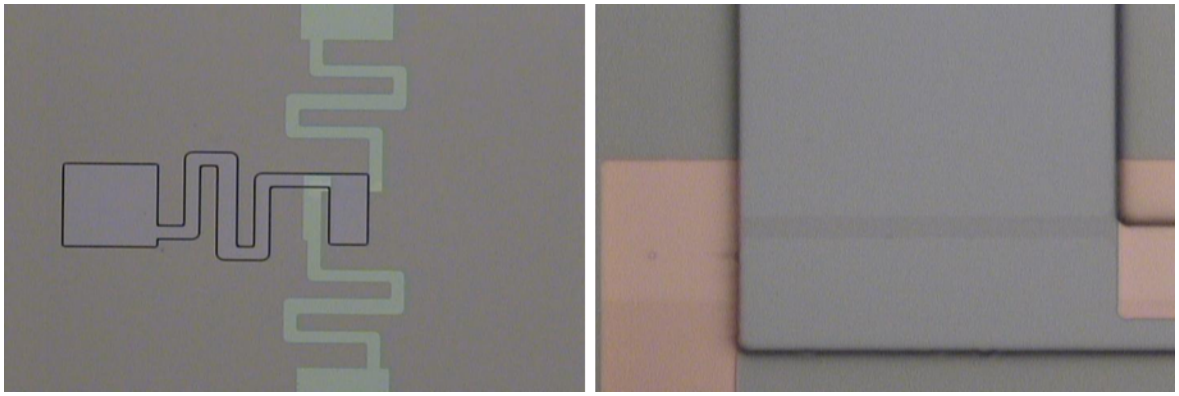

10. Photolithography for forming the patterns of gate-electrodes

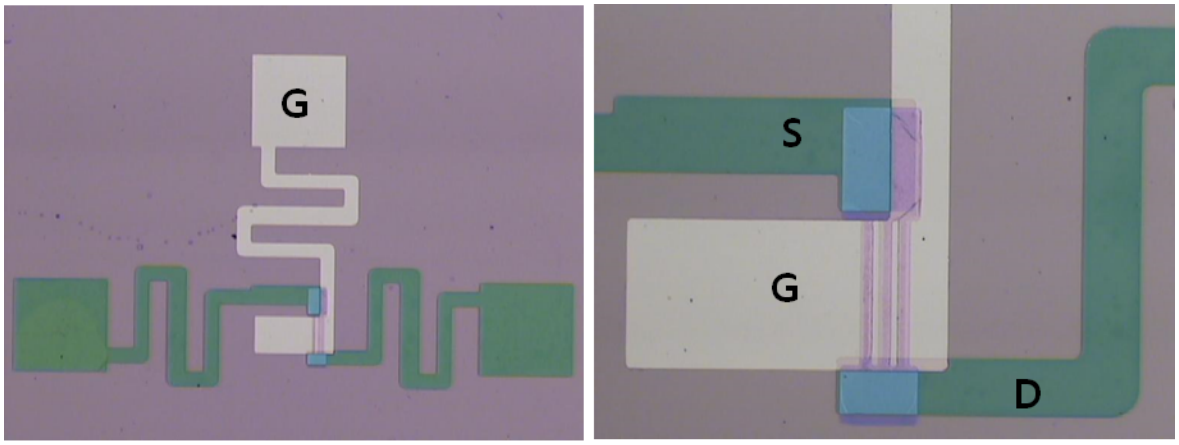

11. E-beam evaporation for forming S-D electrodes (30 nm Au/3 nm Ti)
12. Lift-off

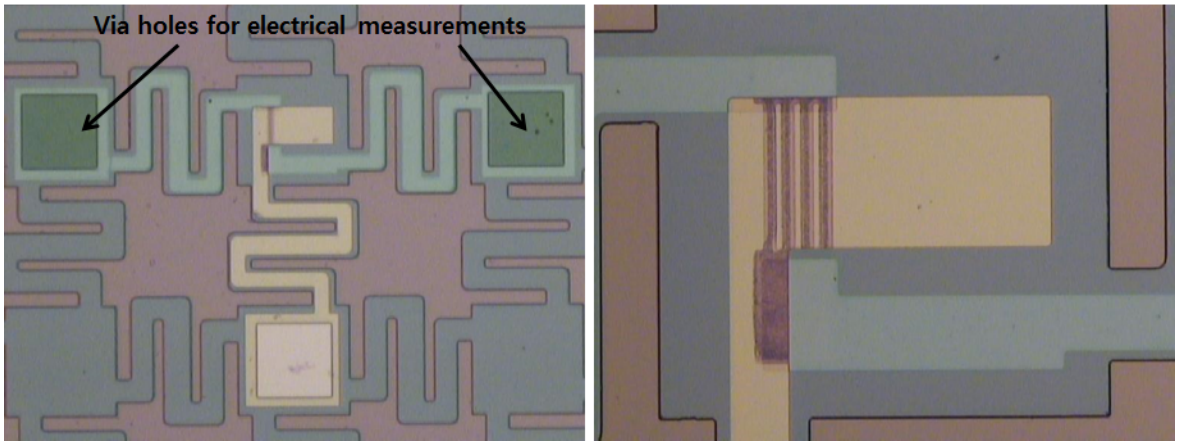

13. Photolithography for the opening of via holes for electrical measurements

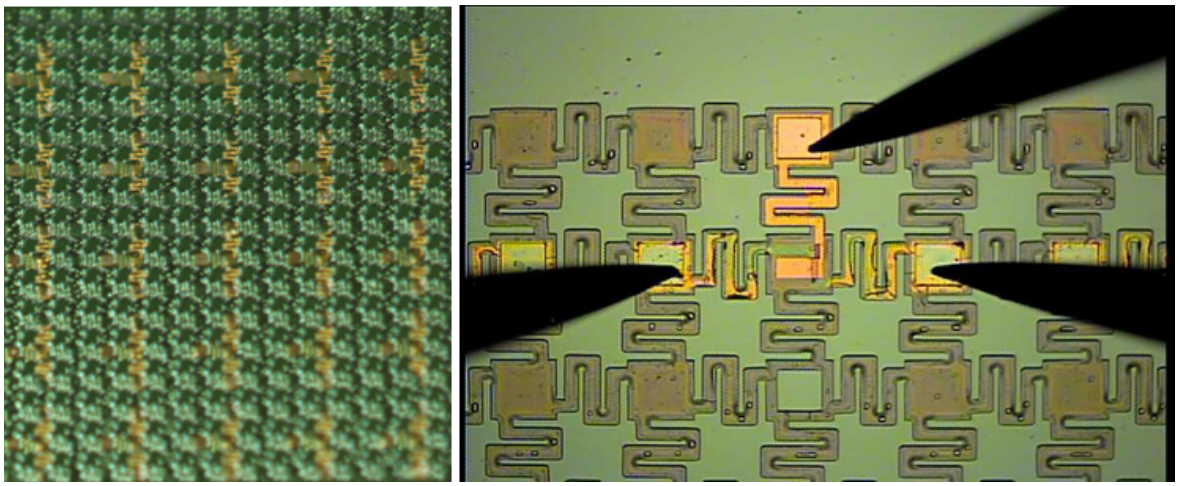

14. Al_2O_3 gate dielectric etching with Al etchant

Raman analysis

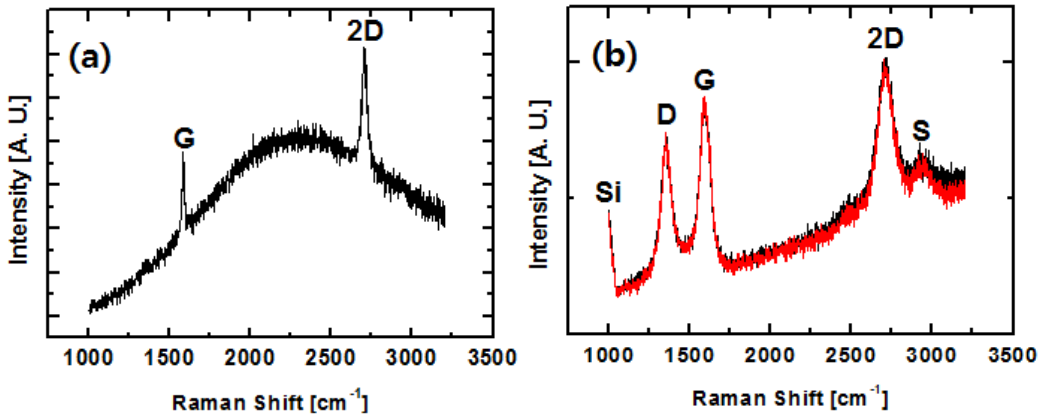

Original Raman spectra taken from (a) the graphene films on Cu foil and (b) the nGr films on Al_2O_3. Si and S mean that second-order Si (111) peak and D+D' peak, respectively.

References

1. S. V. Kusminskiy, D. K. Campbell, A. H. Castro Neto, F. Guinea, *Phys. Rev. B* 2011, **83**, 165405.

2. K. V. Zhkharchenko, M. I. Katsnelson, A. Fasolino, *Phy. Rev. Lett.* 2009, **102**, 046 808.

3. A. Fasolino, J. H. Los, M. I. Katsnelson, *Nature Mater.* 2007, **6**, 858-861.

4. B. Huang, Q. Xu, S.-H. Wei, *Phys. Rev. B* 2011, **84**, 155406.

5. N. T. Cuong, M. Otani, S. Okada, *Phy. Rev. Lett.* 2011, **106**, 106801.

6. J. Sabio, C. Seoánez, S. Fratini, F. Guinea, A. H. Castro Neto, F. Sols, *Phys. Rev. B* 2008, **77**, 195409.

7. P. Avouris, *Nano Lett.* 2010, **10**, 4285-4294.

8. B. Huang, Q. Xu, S.-H. Wei, *Phys. Rev. B* 2011, **84**, 155406.

9. X. Li, X. Wang, L. Zhang, S. Lee, H. Dai, *Science* 2008, **319**, 1229-1232.